Volume 17 | Number 19 | 21 May 2015 | Pages 12371–13162

PCCP

Physical Chemistry Chemical Physics

www.rsc.org/pccp

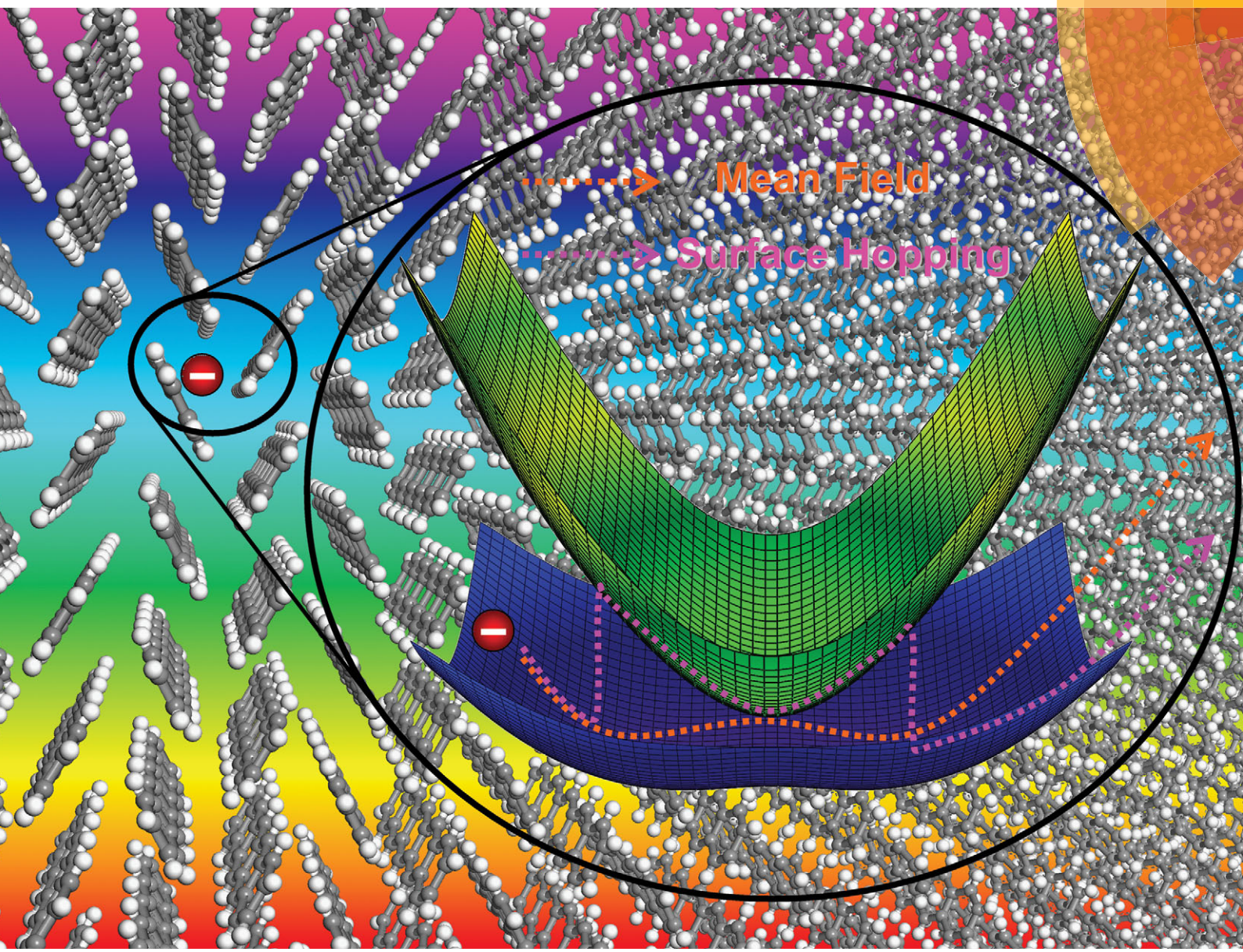

ISSN 1463-9076

ROYAL SOCIETY OF CHEMISTRY

PERSPECTIVE

Linjun Wang, Oleg V. Prezhdo and David Beljonne

Mixed quantum-classical dynamics for charge transport in organics

PCCP

PERSPECTIVE

View Article Online
View Journal | View Issue

Cite this: *Phys. Chem. Chem. Phys.*, 2015, **17**, 12395

Mixed quantum-classical dynamics for charge transport in organics

Linjun Wang,*[a] Oleg V. Prezhdo*[a] and David Beljonne*[b]

Received 26th January 2015,
Accepted 9th March 2015

DOI: 10.1039/c5cp00485c

www.rsc.org/pccp

Charge transport plays a crucial role in the working principle of most opto-electronic and energy devices. This is especially true for organic materials where the first theoretical models date back to the 1950s and have continuously evolved ever since. Most of these descriptions rely on perturbation theory to treat small interactions in the Hamiltonian. In particular, applying a perturbative treatment to the electron–phonon and electron–electron coupling results in the band and hopping models, respectively, the signature of which is conveyed by a characteristic temperature dependence of mobility. This perspective describes recent progress of studying charge transport in organics using mixed quantum-classical dynamics techniques, including mean field and surface hopping theories. The studies go beyond the perturbation treatments and represent the processes explicitly in the time-domain, as they occur in real life. The challenges, advantages, and disadvantages of both approaches are systematically discussed. Special focus is dedicated to the temperature dependence of mobility, the role of local and nonlocal electron–phonon couplings, as well as the interplay between electronic and electron–phonon interactions.

1. Introduction

Semiconductors are everywhere in our life. Silicon has held a dominant position in modern technologies for about forty years. Despite great successes in multiple applications, conventional inorganic electronics will likely reach its limits in the near future and face a number of practical issues that prevent applications, in which cost, mechanical properties, and tenability are important. Organic semiconductors have gained increasing interest over the past few decades.[1] These affordable materials possess many novel advantages, such as light weight, mechanical flexibility, easy fabrication, and large scale production, which can be used to overcome the bottlenecks of their inorganic competitors.[2] To date, organics have found wide applications in various (opto)electronic and energy devices, such as organic field-effect transistors,[3] organic light-emitting diodes,[4] and organic photovoltaics.[5]

The overall efficiency of electronic devices relies strongly on the carrier mobility of functional organic semiconductors. Theoretical studies are very helpful to reveal the intrinsic charge transport mechanism.[6–11] Because of complex electron–phonon couplings (EPCs), charge transport is a many-particle problem, which is extremely difficult to solve. Perturbation theories have been extensively explored, and two well-known regimes for charge transport have been identified.[10] On the one hand, when intermolecular electronic couplings are much weaker than EPCs and treated as a perturbation, charge transport falls into the hopping regime. There, the charge carriers are completely localized on individual molecules and diffuse by hopping from one site to another. The hopping transport is thermally activated, because increasing temperature provides the activation energy for the charge carriers to overcome the barrier associated with both intra- and inter-molecular geometric relaxation. On the other hand, when the EPCs are weak and regarded as a perturbation, the band regime of charge transport is activated. The charge is delocalized over the whole system, and the carrier mobility generally decreases with temperature due to the enhanced phonon scattering. Instead of using free charges as elementary carriers, a more general description is provided in the framework of the so-called polaron model,[12–15] where the charge carrier moves together with the dressed phonon cloud and behaves as a quasi-particle named polaron. The coupling between polarons is normally treated as a perturbation, and the two distinct charge transport regimes can be reproduced.[16,17] In general cases, however, no parameter can be easily treated as a perturbation, and thus non-perturbative methods are in demand.

Due to the different nature of electrons and nuclei involved in charge transport, only the former should be dealt with quantum mechanically, while the later can be treated more simply, in a classical manner. As a result, charge transport can be described with a mixed quantum-classical dynamics (MQCD) idea,[8,9] which has attracted growing interest in many

[a] *Department of Chemistry, University of Southern California, Los Angeles, CA 90089-0482, USA. E-mail: linjun.wang@usc.edu, prezhdo@usc.edu*
[b] *Laboratory for Chemistry of Novel Materials, University of Mons, Place du Parc 20, B-7000, Mons, Belgium. E-mail: david.beljonne@umons.ac.be*

other research fields as well, *e.g.*, proton transfer,[18] exciton dynamics,[19] and vibrational relaxation.[20] MQCD has two major flavors: mean field (MF) (also known as Ehrenfest)[21,22] and surface hopping (SH),[23,24] both of which are non-perturbative. They share the same feature that the electronic state responds instantaneously to the nuclear motion. The difference resides primarily in the description of the classical equations of motion (EOM) for the nuclei. In the MF theory, they are governed by the gradient of the expectation value of the system energy, namely, a single average potential energy surface (PES). In contrast, by design, the SH method incorporates nonadiabatic transitions between different PESs. As a result, SH is more appropriate when nuclear evolution on different PESs may lead to divergent trajectories.

In this Perspective, we bring together recent MQCD studies devoted to charge transport in organics. We begin by reviewing the widely used model Hamiltonians designed to cover different types of EPCs. The MF and SH methods for charge transport are then discussed in detail. Special focus is given to the insights into the charge transport mechanisms obtained from the MF and SH theories. The theories are evaluated in both band and hopping regimes using analytical results as reference. Available numerical calculations for realistic materials are also examined. Finally, we conclude with an outlook for the future of MQCD in application to design of organic materials with desired charge transport properties.

2. Modeling charge transport with mixed quantum-classical techniques

The theories described in this section are based on minimal model Hamiltonians for typical organic materials, but can be easily extended for more complex Hamiltonians to investigate charge transport in realistic materials.

2.1 Hamiltonian

One-dimensional molecular stacks characterized by Su–Schrieffer–Heeger (SSH)-type Hamiltonians[25] are widely used to investigate the charge transport properties in organic materials.[26–31] In practice, an array of N molecular sites with periodic boundary conditions and equal spacing between all nearest neighbors, L, are considered. Without loss of generality and to simplify the formulations, each molecule k is associated with one electronic orbital $|k\rangle$ (*e.g.*, the highest occupied molecular orbital, HOMO, for hole transport and the lowest unoccupied molecular orbital, LUMO, for electron transport) and one intramolecular harmonic vibrational degrees of freedom, x_k (the corresponding velocity is v_k) with the same force constant, K, and effective mass, m. At equilibrium geometry, the onsite energies of all molecules are identical and are therefore set to zero for simplicity. Because the intermolecular electronic coupling, which is proportional to the overlap between molecular orbitals, is short-range in nature, a tight-binding model is widely used to characterize molecular systems. The electronic couplings between all nearest neighbors at equilibrium are the same and assigned to be $-\tau$. Note that such a minimum model for charge transport can be easily generalized to more complex cases with higher space dimension, static disorder, external electric field, and multiple electronic orbitals or vibrational modes per molecular site.

If the onsite energy of molecule k is linearly modulated by x_k, namely, the system experiences local EPCs, the Hamiltonian reads,[28]

$$H_{\text{local}} = \sum_k \alpha x_k |k\rangle\langle k| + \sum_k -\tau(|k\rangle\langle k+1| + |k+1\rangle\langle k|) + \sum_k \frac{1}{2}\left(m{v_k}^2 + K{x_k}^2\right), \quad (1)$$

where α is the local EPC constant. Alternatively, if the electronic coupling between molecule k and its neighboring molecule $k+1$ is linearly modulated by the intermolecular displacement $x_{k+1} - x_k$, the resulting Hamiltonian incorporating such nonlocal EPCs can be written as

$$H_{\text{nonlocal}} = \sum_k [-\tau + \beta(x_{k+1} - x_k)](|k\rangle\langle k+1| + |k+1\rangle\langle k|) + \sum_k \frac{1}{2}\left(m{v_k}^2 + K{x_k}^2\right), \quad (2)$$

where β is the nonlocal EPC constant. Apparently, a more general Hamiltonian can be constructed considering both local and nonlocal EPCs,

$$H_{\text{general}} = \sum_k \alpha x_{1,k}|k\rangle\langle k| + \sum_k \left[-\tau + \beta\left(x_{2,k+1} - x_{2,k}\right)\right](|k\rangle\langle k+1| + |k+1\rangle\langle k|) + \sum_k \frac{1}{2}\left(m_1 {v_{1,k}}^2 + K_1 {x_{1,k}}^2\right) + \sum_k \frac{1}{2}\left(m_2 {v_{2,k}}^2 + K_2 {x_{2,k}}^2\right). \quad (3)$$

Here two vibrational degrees of freedom are considered for each molecule. In the following context, eqn (1)–(3) will be abbreviated as the local, nonlocal, and general Hamiltonians, respectively.

2.2 Mean field theory

The time evolution of the wave function, $\psi(t)$, is generally described by the time-dependent Schrödinger equation,

$$\dot{\psi}(t) = H\psi(t)/i\hbar. \quad (4)$$

At the MF level, the acceleration of any classical degree of freedom is obtained through the spatial derivative of the expectation value of the system energy,

$$\dot{v}_k = -\frac{1}{m}\frac{\partial\langle\psi(t)|H|\psi(t)\rangle}{\partial x_k}. \quad (5)$$

If $\psi(t)$ is expressed as a linear expansion of the basis states, $\{|k\rangle\}$,

$$\psi(t) = \sum_k \psi_k(t)|k\rangle, \quad (6)$$

we can easily obtain the following EOM based on the general Hamiltonian given by eqn (3),[30]

$$\begin{aligned}\dot{\psi}_k &= -\frac{\tau}{i\hbar}(\psi_{k+1}+\psi_{k-1}) + \frac{\alpha}{i\hbar}x_{1,k}\psi_k \\ &\quad + \frac{\beta}{i\hbar}\left[(x_{2,k+1}-x_{2,k})\psi_{k+1} + (x_{2,k}-x_{2,k-1})\psi_{k-1}\right],\end{aligned} \tag{7}$$

$$\dot{v}_{1,k} = (-K_1 x_{1,k} - \alpha\psi_k^*\psi_k)/m_1, \tag{8}$$

$$\dot{v}_{2,k} = [-K_2 x_{2,k} + \beta(\psi_k^*\psi_{k+1} + \psi_{k+1}^*\psi_k - \psi_{k-1}^*\psi_k - \psi_k^*\psi_{k-1})]/m_2. \tag{9}$$

By means of these differential EOM, all the relevant dynamical quantities (*i.e.*, ψ_k, $v_{1,k}$, $v_{2,k}$, $x_{1,k}$, and $x_{2,k}$) can be solved iteratively by the standard fourth-order Runge–Kutta (RK4) algorithm.[32] Note that there also exists explicit integrators designed specifically for MQCD.[33]

The above MF calculations can be also carried out *via* the density matrix,

$$\rho(t) = \sum_{kl}\rho_{kl}(t)|k\rangle\langle l|. \tag{10}$$

The time derivative of the density matrix is obtained through the Liouville equation,

$$\dot{\rho}(t) = [H(t),\rho(t)]/i\hbar, \tag{11}$$

and the classical acceleration becomes

$$\dot{v}_k(t) = -\frac{1}{m}\frac{\partial \mathrm{Tr}[H(t)\rho(t)]}{\partial x_k}, \tag{12}$$

Based on the general Hamiltonian, it's easy to obtain[28]

$$\begin{aligned}\dot{\rho}_{kl} &= -\frac{\tau}{i\hbar}(\rho_{k+1,l}+\rho_{k-1,l}-\rho_{k,l-1}-\rho_{k,l+1}) + \frac{\alpha}{i\hbar}(x_{1,k}-x_{1,l})\rho_{kl} \\ &\quad + \frac{\beta}{i\hbar}\left[(x_{2,k+1}-x_{2,k})\rho_{k+1,l} + (x_{2,k}-x_{2,k-1})\rho_{k-1,l}\right] \\ &\quad - \frac{\beta}{i\hbar}\left[(x_{2,l}-x_{2,l-1})\rho_{k,l-1} + (x_{2,l+1}-x_{2,l})\rho_{k,l+1}\right],\end{aligned} \tag{13}$$

$$\dot{v}_{1,k} = (-K_1 x_{1,k} - \alpha\rho_{kk})/m_1, \tag{14}$$

$$\dot{v}_{2,k} = [-K_2 x_{2,k} + 2\beta(\mathrm{Re}\rho_{k,k+1} - \mathrm{Re}\rho_{k,k-1})]/m_2. \tag{15}$$

Analogously, the time evolution of ρ_{kl}, $v_{1,k}$, $v_{2,k}$, $x_{1,k}$, and $x_{2,k}$ can be solved iteratively by RK4.[32] Besides, it's straightforward that the wave function approach based on eqn (4)–(9) and density matrix approach described by eqn (10)–(15) are fully equivalent at the MF level.[28]

2.3 Initial conditions

To calculate the charge carrier mobility, one needs to carry out a series of simulations with different initial conditions to characterize the canonical ensemble of nuclear degrees of freedom. For a harmonic oscillator, it is well-known that the nuclear position follows a Gaussian distribution,[31,34]

$$P(x) = \frac{1}{\sigma_x\sqrt{2\pi}}\mathrm{e}^{-x^2/2\sigma_x{}^2}. \tag{16}$$

The variance of the nuclear position is

$$\sigma_x{}^2 = \frac{\hbar}{2\sqrt{Km}}\coth\left(\frac{\hbar\omega}{2k_\mathrm{B}T}\right). \tag{17}$$

where $\hbar$ is the reduced Planck constant, $\omega = (K/m)^{1/2}$ is the vibrational frequency, k_B is the Boltzmann constant, and T is the system temperature. In the low temperature (high frequency) limit, eqn (17) goes to

$$\sigma_x{}^2 = \frac{\hbar}{2\sqrt{Km}}, \tag{18}$$

which is independent of temperature, representing the coordinate uncertainty of ground state nuclear vibration. And in the high temperature (low frequency) limit, eqn (17) becomes

$$\sigma_x{}^2 = \frac{k_\mathrm{B}T}{K}, \tag{19}$$

which is actually the classical Boltzmann distribution. Similarly, the variance for nuclear momentum is expressed as,

$$\sigma_p{}^2 = \frac{\hbar\sqrt{Km}}{2}\coth\left(\frac{\hbar\omega}{2k_\mathrm{B}T}\right). \tag{20}$$

In MQCD, nuclear vibrations are treated classically. According to the Boltzmann distribution, the initial $\{x_{1,k}\}$, $\{x_{2,k}\}$, $\{v_{1,k}\}$, and $\{v_{2,k}\}$ can be set as Gaussian random numbers with variance $k_\mathrm{B}T/K_1$, $k_\mathrm{B}T/K_2$, $k_\mathrm{B}T/m_1$, and $k_\mathrm{B}T/m_2$, respectively. Using eqn (17) and (20) instead as initial conditions, one can achieve a better description of charge transport at low temperatures. In addition, the equilibrium geometry for nuclear vibrations should be also taken into account to setup the initial conditions.[30] Based on the local Hamiltonian in eqn (1), the neutral molecular geometries ($x_k = 0$) are generally used. This is reasonable for systems falling in the band regime, but is questionable in the hopping regime with low mobility, where the presence of a charge is accompanied by a distortion of the molecular structure. When the charge is localized on a single molecule, the charged geometry of the corresponding molecule is associated with $x_k = -\alpha/K$.[30]

2.4 Charge carrier mobility

For each realization m, the corresponding time-dependent wave function $\psi^{(m)}(t)$ or density matrix $\rho^{(m)}(t)$ can be obtained. The mean squared displacement (MSD) is then calculated by[28]

$$\mathrm{MSD}(t) = \frac{1}{M}\sum_{m=1}^{M}\left[\left\langle\psi^{(m)}(t)\middle|r^2\middle|\psi^{(m)}(t)\right\rangle - \left\langle\psi^{(m)}(t)\middle|r\middle|\psi^{(m)}(t)\right\rangle^2\right], \tag{21}$$

and

$$\mathrm{MSD}(t) = \frac{1}{M}\sum_{m=1}^{M}\left\{\mathrm{Tr}\left[\rho^{(m)}(t)r^2\right] - \mathrm{Tr}^2\left[\rho^{(m)}(t)r\right]\right\}, \tag{22}$$

using the wave function and density matrix approaches, respectively. M is the total number of realizations. When/if the MSD shows a linear evolution in time, one enters the regime of

equilibrium diffusion and the diffusion coefficient is evaluated through the time derivative of the MSD as

$$D = \frac{1}{2n}\lim_{t\to\infty}\frac{\mathrm{dMSD}}{\mathrm{d}t}. \tag{23}$$

where n is the space dimension (*e.g.*, $n = 1$ for one-dimensional systems). Finally, the carrier mobility can be calculated by means of the Einstein relation,[35,36]

$$\mu = \frac{e}{k_\mathrm{B}T}D. \tag{24}$$

where e is the elementary charge.

2.5 Mean field theory without feedback

As shown in eqn (7)–(9) and (13)–(15), the combined dynamics of electrons and nuclei should be solved self-consistently, that is to say, electron evolution has an impact on nuclear dynamics and *vice versa*. When electron dynamics is ultrafast in comparison with the nuclear energy relaxation, its influence on nuclear vibrations can be neglected.[28] As a result, eqn (8), (9), (14) and (15) simply reduce to

$$\dot{v}_{1,k} = -K_1 x_{1,k}/m_1, \tag{25}$$

$$\dot{v}_{2,k} = -K_2 x_{2,k}/m_2, \tag{26}$$

which correspond to the EOM for isolated harmonic oscillators in the absence of feedback from the electron to nuclei. This approximation offers great advantages when studying charge transport properties in realistic materials.[28] In detail, one can perform molecular dynamics simulations to get a set of realizations of nuclear trajectories, and use quantum-chemical single point calculations to get the corresponding time-dependent electronic Hamiltonian for each realization. The time-dependent wave function and density matrix can then be obtained through eqn (7) and (13), respectively. Finally, the charge transport mobility can be evaluated by eqn (21)–(24).

2.6 Surface hopping method

SH in the adiabatic representation usually gives more accurate results than that in the diabatic representation.[37,38] However, there exists great difficulty to implement SH formalisms for charge transport in large molecular systems mostly due to the existence of high density of adiabatic PESs.[29,39] Intermolecular electronic couplings are weak and short-range interactions. Most crossings happen between localized adiabatic states that are far away, and have no contribution to the charge transport process. Accurately dealing with these massive trivial crossings is quite difficult. Recently, a flexible surface hopping (FSH) technique,[29] which treats only a small portion of the system in a SH manner and does it in a flexible way in time, has been proposed. In this QM/MM-like approach, the problematic crossing problem is avoided because all adiabatic states are spatially close and the computational cost is largely reduced because only a small Hamiltonian matrix is diagonalized to get all important PESs. A flexible time step technique, which ensures the smoothness of all time-dependent adiabatic states, was proposed, to enable an accurate SH description with the largest possible time intervals.

In detail, diagonalizing the Hamiltonian, one gets the adiabatic states in terms of the original diabatic orbitals, $\left\{\Phi_i = \sum_k p_{ki}|k\rangle\right\}$, and the corresponding energies, $\{E_i\}$, to construct the adiabatic PESs. The electron wave function is defined as a linear expansion of these adiabatic states, *i.e.*, $\Phi = \sum_i c_i\Phi_i$. According to the Schrödinger equation, one obtains[29]

$$\dot{c}_i = \frac{1}{i\hbar}c_i E_i - \sum_{j\neq i} c_j \sum_k \left(\dot{x}_{1,k} d_{ij}^{1,k} + \dot{x}_{2,k} d_{ij}^{2,k}\right), \tag{27}$$

where

$$d_{ij}^{1(2),k} = \left\langle \Phi_i \middle| \frac{\mathrm{d}}{\mathrm{d}x_{1(2),k}} \middle| \Phi_j \right\rangle, \tag{28}$$

are nonadiabatic couplings. The nuclear EOM are modeled by the Langevin equation,

$$m_{1(2)}\ddot{x}_{1(2),k} = -V_{1(2),k}{}' - \gamma m_{1(2)}\dot{x}_{1(2),k} + \xi_{1(2)}, \tag{29}$$

Here, $V_{1(2),k}{}' = K_{1(2)}x_{1(2),k} + \mathrm{d}E_a/\mathrm{d}x_{1(2),k}$, with a representing the active adiabatic surface, γ is the fraction coefficient characterizing system-bath coupling strength, $\xi_{1(2)}$ is a Markovian Gaussian random force with standard deviation $(2\gamma m_{1(2)}k_\mathrm{B}T/\Delta t)^{1/2}$, and Δt is the time interval. The differential equations, eqn (27) and (29), can be solved with the RK4 method.[32,40] The Langevin equation like eqn (29) can be also solved with the numerical integration method introduced by Ermak and Buckholz.[41] Based on the Hellmann–Feynman theorem,[42] we obtain[29]

$$d_{ij}^{1,k} = \frac{\alpha p_{ki}p_{kj}}{E_j - E_i}, \tag{30}$$

$$d_{ij}^{2,k} = \frac{\beta\left[p_{ki}\left(p_{k-1,j} - p_{k+1,j}\right) + p_{kj}\left(p_{k-1,i} - p_{k+1,i}\right)\right]}{E_j - E_i}, \tag{31}$$

$$\frac{\mathrm{d}E_i}{\mathrm{d}x_{1,k}} = \alpha {p_{ki}}^2, \tag{32}$$

$$\frac{\mathrm{d}E_i}{\mathrm{d}x_{2,k}} = 2\beta p_{ki}\left(p_{k-1,i} - p_{k+1,i}\right), \tag{33}$$

$$\frac{\mathrm{d}^2E_i}{\mathrm{d}{x_{1,k}}^2} = 2\alpha\sum_{j\neq i} d_{ji}^{1,k}p_{ki}p_{kj}, \tag{34}$$

$$\frac{\mathrm{d}^2E_i}{\mathrm{d}{x_{2,k}}^2} = 2\beta\sum_{j\neq i} d_{ji}^{2,k}\left[p_{ki}\left(p_{k-1,j} - p_{k+1,j}\right) + p_{kj}\left(p_{k-1,i} - p_{k+1,i}\right)\right]. \tag{35}$$

The active SH subsystem is free to self-adjust during the charge transport process, through adding and/or removing neighboring molecules to/from the subsystem at each time step. For example, in order to check whether a molecular orbital $|j\rangle$ should be added or not, we regard the active state of the SH subsystem $\left(\Phi_a = \sum_i p_{ia}|i\rangle\right)$ and this test state

together as a two-level system. Their onsite energies and coupling are[29]

$$\langle \Phi_a|H|\Phi_a\rangle = \alpha \sum_i {p_{ia}}^2 x_{1,i} + \sum_i 2\left[-\tau + \beta\left(x_{2,i+1} - x_{2,i}\right)\right] p_{i+1,a} p_{ia}, \tag{36}$$

$$\langle j|H|j\rangle = \alpha x_{1,j}, \tag{37}$$

$$\begin{aligned}\langle \Phi_a|H|j\rangle \;&= \alpha p_{ja} x_{1,j} + \left[-\tau + \beta\left(x_{2,j+1} - x_{2,j}\right)\right] p_{j+1,a} \\ &\quad + \left[-\tau + \beta\left(x_{2,j} - x_{2,j-1}\right)\right] p_{j-1,a}.\end{aligned} \tag{38}$$

When the ratio between the absolute coupling, abs$\{\langle \Phi_a|H|j\rangle\}$, and the absolute energy difference, abs$\{\langle \Phi_a|H|\Phi_a\rangle - \langle j|H|j\rangle\}$, is larger than a critical fraction R_c, $|j\rangle$ is added into the new subsystem for SH. Similar procedures are carried out when removing a molecular orbital from the SH subsystem. Meanwhile, the new active state is set as the adiabatic state of the new subsystem which mostly overlaps with the old active state. Obviously, this approach converges to the traditional SH when R_c goes to 0, while alleviating the trivial crossing problem at finite R_c.[29] In addition, a proper Δt can be adjusted at each time step to ensure that the minimum overlap between the adiabatic state at time t and the corresponding state at the next time step $t + \Delta t$, $\min\{|\langle \Phi_i(t)|\Phi_i(t+\Delta t)\rangle|\}$, is always higher than a critical value O_c. Note that smaller time steps are automatically generated when the dynamics approaches nonadiabatic regimes to prevent the divergence of eqn (30) and (31). As in Tully's fewest switches surface hopping (FSSH) algorithm, the switching probability from the active surface i to another surface j is[23]

$$g_{ij} = \max\left\{0, \frac{2\Delta t \mathrm{Re}\left[c_i c_j^* \sum_k \left(v_{1,k} d_{ij}^{1,k} + v_{2,k} d_{ij}^{2,k}\right)\right]}{c_i^* c_i}\right\}. \tag{39}$$

When a surface hop to j-th PES is chosen stochastically, one needs to ensure that $E_i + \sum_k \left(m_1 {v_{1,k}}^2 + m_2 {v_{2,k}}^2\right)/2 > E_j$ and adjust nuclear velocities along the direction of the nonadiabatic coupling vector to conserve the total energy,[29]

$${v_{1(2),k}}' = v_{1(2),k} + d_{ij}^{1(2),k} \frac{A}{B}\left[\sqrt{1 + 2\left(E_i - E_j\right)\frac{B}{A^2}} - 1\right]. \tag{40}$$

where

$$A = \sum_k m_1 v_{1,k} d_{ij}^{1,k} + \sum_k m_2 v_{2,k} d_{ij}^{2,k}, \tag{41}$$

$$B = \sum_k m_1 \left(d_{ij}^{1,k}\right)^2 + \sum_k m_2 \left(d_{ij}^{2,k}\right)^2. \tag{42}$$

If $E_i + A^2/(2B) < E_j$, the hop is rejected; otherwise, the trajectory evolves on the PES E_j. Environmental fluctuations tend to destruct the superpositioned quantum states, resulting in coherence loss. Decoherence effects can be naturally considered through damping off-diagonal terms of the density matrix with pairwise decoherence rates.[43] The simplest way to implement decoherence can be achieved by collapsing the electronic wave function to the new PES after every successful and unsuccessful hop.[44] For each realization m, the time evolution of the active state $\Phi_a^{(m)}(t)$ is restored and used to calculate the MSD after a total number of M realizations,

$$\mathrm{MSD}(t) = \frac{1}{M}\sum_{m=1}^{M}\left[\left\langle \Phi_a^{(m)}(t)\middle|r^2\middle|\Phi_a^{(m)}(t)\right\rangle - \left\langle \Phi_a^{(m)}(t)\middle|r\middle|\Phi_a^{(m)}(t)\right\rangle^2\right]. \tag{43}$$

The carrier mobility is calculated through the Einstein relation in eqn (24).

2.7 Surface hopping without feedback

Similar to the MF case discussed previously in Section 2.5, the feedback from electron dynamics to nuclear vibrations can also be neglected in certain limits, resulting the so-called classical path approximation (CPA).[45] Such an approximation assumes that the classical trajectory is independent of electron dynamics, while it is not the case the other way round. CPA is appropriate when the nuclear thermal energy is much greater than the electronic activation energy, that is, the energy exchange between electrons and nuclei does not have a strong impact on the nuclear dynamics. Due to the stochastic nature of SH methods, a large number of realizations are required to get converged results, making the computational cost extremely high particularly for a first-principle study of large systems. Charge transport calculations at the CPA level utilize either force field or *ab initio* molecular dynamics to obtain only one pre-computed nuclear trajectory, along which a series of SH simulations are performed to obtain the carrier mobility. The computational cost is significantly reduced, and thus larger system size and/or longer time scale can be reached. So far available surface hopping investigations for charge transport in realistic materials are mostly carried out with CPA.[46] To mimic the hop rejection due to the violation of energy conservation, the surface hopping probabilities in eqn (39) are rescaled by the Boltzmann factor to account the detailed balance,[45]

$$g_{ij} = \max\left\{0, \frac{2\Delta t \mathrm{Re}\left[c_i c_j^* \sum_k \left(v_{1,k} d_{ij}^{1,k} + v_{2,k} d_{ij}^{2,k}\right)\right]}{c_i^* c_i}\right\} b_{ij}, \tag{44}$$

where

$$b_{ij} = \begin{cases} \exp\left(-\dfrac{E_j - E_i}{k_B T}\right), & E_j > E_i. \\ 1, E_j \le E_i \end{cases} \tag{45}$$

The processes to calculate the carrier mobility remains the same.

3. Results and discussion

3.1 Charge transport with mean field theory

The MF theory is the most widely used MQCD technique for charge transport studies so far. A lot of new insights have been obtained and will be extensively discussed in the following subsections.

3.1.1 Role of initial charge extension on equilibrium transport. Charge carrier mobility is a steady state property, and thus should be insensitive to the choice of initial charge distribution. As an illustration, the initial population has been equally distributed over a certain number of contiguous molecules in a linear stack, and its role on the time dependence of MSD has been examined based on the nonlocal Hamiltonian.[28] As shown in Fig. 1, the time-dependent MSD with different initial charge extension differs significantly within the first several ps, but the time evolutions become more or less parallel to each other at longer time scale. As a result, the corresponding dMSD/dt (and thus the charge carrier mobility) converges to the same value eventually. The convergence with simulation time is found to be faster for smaller initial charge extension. Similar observations also hold for the local Hamiltonian. In general cases, therefore, one can initially localize the charge on a single molecular site to reduce the total simulation time for equilibrium charge transport.

3.1.2 Feedback from electron dynamics to nuclear vibrations. If the feedback from the quantum charge carriers on the classical nuclei can be completely neglected, a multiscale simulation approach can be naturally constructed, taking the advantage of molecular dynamics for nuclear trajectories, quantum chemical calculations for the time-dependent Hamiltonian, and MQCD simulations for charge transport properties. It is thus of great interest to study how feedback effects depend on details of the Hamiltonian. Due to the different nature of local and nonlocal EPCs, the feedback effect can be investigated separately as follows.

For the local Hamiltonian, numerical calculations have been carried out for one-dimensional stacks in a broad parameter space.[28] For each data point, the converged dMSD/dt values obtained by either treating electron–phonon interactions explicitly or neglecting the feedback from electron dynamics to nuclear vibrations have been compared. As shown in Fig. 2, when $(\mathrm{dMSD/d}t)_{\mathrm{Ehrenfest}}$ is larger than $0.1L^2$ fs^{-1}, $(\mathrm{dMSD/d}t)_{\mathrm{approx}}$ is almost identical to $(\mathrm{dMSD/d}t)_{\mathrm{Ehrenfest}}$, and thus the feedback effect can be safely neglected. However, the characteristic ratio $(\mathrm{dMSD/d}t)_{\mathrm{approx}}/(\mathrm{dMSD/d}t)_{\mathrm{Ehrenfest}}$ increases up to 1.5 with the decrease of $(\mathrm{dMSD/d}t)_{\mathrm{Ehrenfest}}$. As a result, the carrier mobility

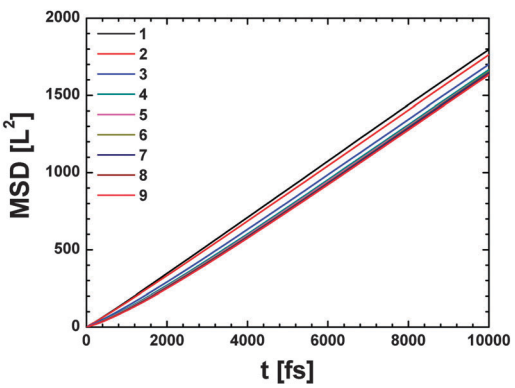

Fig. 1 Time-dependent MSD with different initial charge extension ranging from 1 to 9 molecular sites. The nonlocal Hamiltonian in eqn (2) is chosen with the parameters: τ = 300 cm^{-1}, β = 995 cm^{-1} Å^{-1}, K = 14 500 amu ps^{-2}, m = 250 amu, and T = 150 K, and the wave function strategy of the MF theory is adopted. Reprinted with permission from ref. 28.

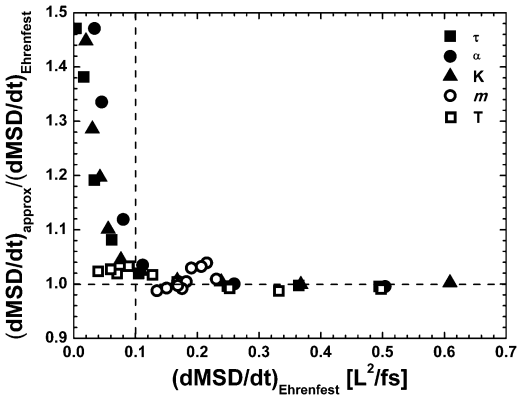

Fig. 2 The ratio of the approximated dMSD/dt without considering the feedback from the charge carrier to the nuclei, $(\mathrm{dMSD/d}t)_{\mathrm{approx}}$, and the Ehrenfest solution of dMSD/dt considering such feedback, $(\mathrm{dMSD/d}t)_{\mathrm{Ehrenfest}}$, as a function of $(\mathrm{dMSD/d}t)_{\mathrm{Ehrenfest}}$ in one-dimensional stacks based on the local Hamiltonian in eqn (1). For each calculation, either the intermolecular electronic coupling (τ), the local EPC (α), the force constant (K), the mass of nuclear vibrations (m), or the temperature (T) is changed, while keeping the other parameters to their reference values (τ = 300 cm^{-1}, α = 3500 cm^{-1} Å^{-1}, K = 14 500 amu ps^{-2}, m = 250 amu, and T = 150 K). The density matrix approach of the MF theory is applied. The dashed lines are used to guide the eyes. Reprinted with permission from ref. 28.

obtained by neglecting the quantum forces on the nuclei can be regarded as an upper limit. Only the values of τ, α, and K have a strong impact on the error because the charge delocalization relies on the interplay between the electronic coupling, τ, and the reorganization energy, $\lambda = \beta^2/K$,[28] and the feedback forces on the nuclei depends on the associated electron population. If the intermolecular distance, L, is set to 5 Å, which is typical for molecular crystals, the critical room-temperature mobility is calculated to be 4.8 cm^2 V^{-1} s^{-1}. Similar calculations have been performed on two-dimensional lattices, where the critical room-temperature mobility is reduced to 0.14 cm^2 V^{-1} s^{-1}.[28] Considering that high carrier mobilities have been widely observed in molecular crystals,[1] the MF approach without feedback thus provides a reliable tool to investigate the intrinsic transport properties in high-mobility materials, while it captures the upper limit in low-mobility materials.

In the case with only nonlocal EPCs, the nuclear dynamics relies only on $\mathrm{Re}\rho_{kl}$ with odd sum indices, see eqn (15). Applying the Liouville equation in eqn (11) to the identity $\mathrm{Re}\rho_{kl} = (\rho_{kl} + \rho_{lk})/2$ yields[28]

$$\frac{\partial \mathrm{Re}\rho_{kl}}{\partial t} = \frac{\sum_j \left(H_{kj}\mathrm{Im}\rho_{jl} - H_{lj}\mathrm{Im}\rho_{kj}\right)}{\hbar}. \quad (46)$$

For the nonlocal Hamiltonian in eqn (2), eqn (46) becomes

$$\frac{\partial \mathrm{Re}\rho_{kl}}{\partial t} = \frac{H_{k,k-1}\mathrm{Im}\rho_{k-1,l} + H_{k,k+1}\mathrm{Im}\rho_{k+1,l}}{\hbar} - \frac{H_{l,l-1}\mathrm{Im}\rho_{k,l-1} + H_{l,l+1}\mathrm{Im}\rho_{k,l+1}}{\hbar}. \quad (47)$$

In other words, $\partial\mathrm{Re}\rho_{kl}/\partial t$ depends on $\mathrm{Im}\rho_{k-1,l}$, $\mathrm{Im}\rho_{k+1,l}$, $\mathrm{Im}\rho_{k,l-1}$, and $\mathrm{Im}\rho_{k,l+1}$, for which the sum of the two indices is of opposite

parity to that of $\partial \mathrm{Re}\rho_{kl}/\partial t$. Similarly, $\partial \mathrm{Im}\rho_{kl}/\partial t$ involves $\mathrm{Re}\rho_{k-1,l}$, $\mathrm{Re}\rho_{k+1,l}$, $\mathrm{Re}\rho_{k,l-1}$, and $\mathrm{Re}\rho_{k,l+1}$, for which the sum of the two indices is also of opposite parity to that of $\partial \mathrm{Im}\rho_{kl}/\partial t$. The initial ρ is generally a real diagonal matrix, namely, only $\mathrm{Re}\rho_{kl}$ with even sum indices are nonzero. Especially, when the total number of molecules is even, it is easy to deduce that $\mathrm{Re}\rho_{kl}$ with odd sum indices will remain zero forever.[28] As a result, eqn (15) reduces to eqn (26), and the feedback from electron to nuclei is rigorously negligible when the Hamiltonian includes only nonlocal EPCs.

3.1.3 Temperature dependence of mobility. As the only source of disorder to the electronic Hamiltonian, nuclear coordinate fluctuations determine the entire temperature dependence of mobility, which also reflects the underlying charge transport mechanism. In general, two critical temperatures can be defined.[31] The first is $T_{c1} = \hbar\omega/k_B$, below which nuclear quantum effect is important. The second is $T_{c2} = \tau^2 K/(\alpha^2 k_B)$ for the local Hamiltonian and $T_{c2} = \tau^2 K/(2\beta^2 k_B)$ for the nonlocal Hamiltonian. When temperature is above T_{c2}, the fluctuation of the electronic Hamiltonian (*i.e.*, $\alpha\sigma_x$ and $2^{1/2}\beta\sigma_x$ for local and nonlocal Hamiltonians, respectively) becomes significant in comparison to the intermolecular transfer integral, τ, and the perturbation theory becomes invalid. As a result, three charge transport regimes can be commonly identified: quantum regime ($T < T_{c1}$), classical perturbative regime ($T_{c1} < T < T_{c2}$), and regime beyond perturbation ($T > T_{c2}$).[31]

In Fig. 3A, a typical temperature dependence of mobility obtained at the MF level based on the local Hamiltonian is shown.[31] Using classical initial conditions, the MF dynamics gives an almost perfect linear relationship in the log–log plot, which implies that the carrier mobility follows an overall power-law dependence. With quantum initial conditions, the temperature dependence remains the same above 50 K, but the mobility is strongly reduced at lower temperatures. Based on the parameters used, the vibrational frequency is calculated to be about 40 cm^{-1}, corresponding to a critical temperature T_{c1} of 58 K. These numerical calculations thus confirmed that a strong change in the transport behavior happens around T_{c1} because of the nuclear quantum effect. Due to the same reason, for the nonlocal Hamiltonian, the role of the quantum initial conditions remains basically the same (see Fig. 3B). Note that systematic studies using the MF theory for charge transport have been carried out with a broad range of parameters, and similar observations have been always obtained.[27,31]

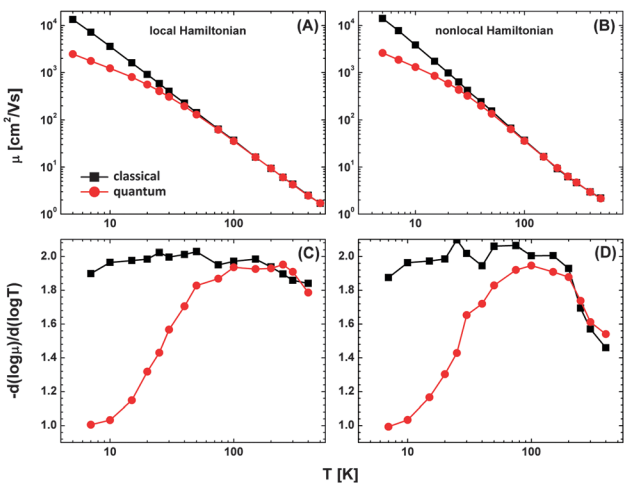

Fig. 3 Temperature dependence of (A) and (B) mobility, μ, and (C) and (D) its derivative, $-\mathrm{d}(\log\mu)/\mathrm{d}(\log T)$, for the MF dynamics with classical and quantum initial conditions. (A) and (C) are based on the local Hamiltonian in eqn (1), while (B) and (D) are based on the nonlocal Hamiltonian in eqn (2). The parameters are chosen as: τ = 300 cm^{-1}, α = 3500 cm^{-1} $\mathrm{Å}^{-1}$, β = 995 cm^{-1} $\mathrm{Å}^{-1}$, K = 14 500 amu ps^{-2}, and m = 250 amu. Reprinted with permission from ref. 31.

The above phenomena can be viewed more clearly when one extracts $n(T) \equiv -\mathrm{d}(\log\mu)/\mathrm{d}(\log T)$ from $\mu(T)$. As shown in Fig. 3C and D, for both local and nonlocal Hamiltonians, the $n(T)$ predicted by the MF theory using classical initial conditions are more or less constant at low temperatures, falling into the classical perturbation regime. Above 150 K, however, they experience an evident reduction. This is related to the transition around T_{c2}, which is calculated to be 128 K for the local Hamiltonian. The decrease of n is even more significant for the nonlocal Hamiltonian. Because the electronic site energies at equilibrium geometries are zero, the fluctuations due to local EPCs always result in a enhancement of electronic disorder and thus a reduction of transport efficiency.[31] It is a different story for nonlocal Hamiltonians, where charge transport relies strongly on the absolute values of transfer integrals. With the increase of temperature, the time-dependent transfer integrals can be of opposite sign of their values at equilibrium geometries.[47] Charge transport can be even relatively enhanced, resulting in a weaker temperature dependence of mobility. The $n(T)$ values calculated with quantum initial conditions are close to unity at extreme low temperatures, falling into the quantum regime. For high temperatures, the results are similar to those using classical initial conditions.

3.1.4 Multiple phonons per molecular site. In realistic organic materials, each molecule is associated with a large number of vibrational modes with different frequencies. The role of multiple phonons has been studied using the local Hamiltonian with two uncorrelated vibrations per molecule.[31] Two sets of calculations with a single vibrational mode and different frequencies are used as references. For systems with local EPCs, the reorganization energy can be calculated as $\lambda = \sum_i \alpha_i^2/K_i$,[28] where i covers all considered vibrational modes. The EPC strengths are adjusted to conserve the total reorganization energy. As shown in Fig. 4, the temperature dependence of mobility using two phonons per molecule falls exactly between the results based on one single phonon per molecule and proper EPCs yielding the same reorganization energy. Thus, the major charge transport mechanism under multiple phonons per molecule can be fully understood with one single vibrational mode as systematically discussed throughout this perspective.

3.2 Assessment of mean field and surface hopping methods

At variance with MF theory that reflects only the average effect of all PESs, the SH method can respond individually to different PESs, and thus has more flexibility to describe complex dynamics

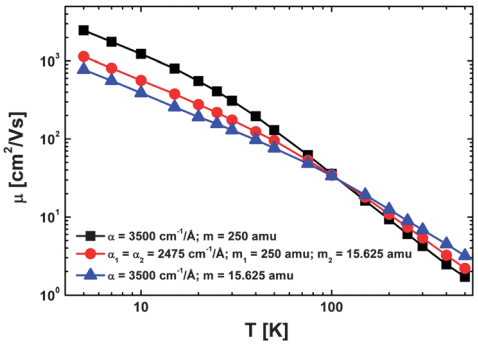

Fig. 4 MF calculated temperature dependence of mobility with either one nuclear vibration (α = 3500 cm^{-1} Å^{-1}, m = 250 amu or m = 15.625 amu) or two nuclear vibrations (α_1 = α_2 = 2475 cm^{-1} Å^{-1}, m_1 = 250 amu, and m_2 = 15.625 amu) coupled to each molecule. The other parameters, τ = 300 cm^{-1} and K = 14 500 amu ps^{-2}, are fixed in all calculations. The local Hamiltonian is used with quantum initial conditions. Reprinted with permission from ref. 31.

like charge transport. In this section, the MF and SH results are benchmarked, and new understandings in charge transport are summarized.

3.2.1 Mean field and surface hopping methods for charge transfer rates. Due to the loose packing between molecules, most organic materials possess weak intermolecular electronic couplings and strong EPCs. In this limit, charge transport falls into the hopping regime, where the whole transport process can be viewed as a series of charge transfer steps between molecular dimers.[7] Analytical rate expressions can be derived from perturbation theories, including the fully quantum mechanical Fermi's golden rule (FGR)[48] and the classically approximated Marcus formula,[49] and further used as references to assess MQCD studies.

In organic semiconductors comprising a single type of conjugated molecules, charge transfer processes between adjacent molecules are actually self-exchange reactions. For simplicity, only one reaction coordinate, x, is considered. The spin-boson Hamiltonian in the basis of diabatic states reads,[30,50]

$$H = \begin{pmatrix} m\omega^2 x^2/2 + Mx & -\tau \\ -\tau & m\omega^2 x^2/2 - Mx \end{pmatrix}, \quad (48)$$

which is actually a special case of the local Hamiltonian given by eqn (1) for two molecular sites. m and ω are the mass and frequency of the nuclear vibration along the reaction path x, respectively. The local EPC factor, M, can be expressed in terms of the reorganization energy, λ, as $M = (\lambda m\omega^2/2)^{1/2}$.[50]

When the perturbation theory is applied in the small electronic coupling limit ($\tau \ll \lambda$), the charge transfer rate is analytically expressed by FGR as[48]

$$k_{\mathrm{FGR}} = \frac{\tau^2}{\hbar^2}\int_{-\infty}^{\infty} \mathrm{d}t \exp\left\{-S\left[(2n+1) - n\mathrm{e}^{-i\omega t} - (n+1)\mathrm{e}^{i\omega t}\right]\right\}, \quad (49)$$

where $n = 1/[\exp(\hbar\omega/k_{\mathrm{B}}T) - 1]$ is the phonon occupation number at temperature T, and $S = \lambda/(\hbar\omega)$ is the Huang-Rhys factor. In the strong coupling ($S \gg 1$) and high temperature ($k_{\mathrm{B}}T \gg \hbar\omega$) limits, eqn (49) naturally reduces to the Marcus rate,[49]

$$k_{\mathrm{Marcus}} = \frac{\tau^2}{\hbar}\sqrt{\frac{\pi}{\lambda k_{\mathrm{B}}T}}\exp\left(-\frac{\lambda}{4k_{\mathrm{B}}T}\right). \quad (50)$$

As a result, a thermally activated temperature dependence of charge transfer rate is generally obtained.

Using existing analytical expressions as references, the performance of the MF and SH theories for charge transfer dynamics has been carefully examined with the temperature dependence as a marker.[30] As mentioned above, the vibrational frequency of 40 cm^{-1} means that the quantum effect in the nuclear motion can be fully neglected above 50 K. As a result, Marcus rates are very close to FGR results for the whole temperature range investigated (see Fig. 5). In line with these temperature-dependent results, SH with or without decoherence give almost identical rates, showing that the decoherence effect is not significantly relevant with the chosen parameters. The MF method with system-bath interaction is found to work surprisingly well, deviating only very slightly from the SH results. The most obvious difference is obtained with the MF theory, where the rate decreases with temperature, in strong contrast with all other approaches.

3.2.2 Mean field and surface hopping methods for charge transport mobilities. Taking the advantage of FGR and Marcus charge transfer rates, the hopping mobility of charge carriers in organic solids can be well-described by the Pauli master equation (PME)[51] or the kinetic Monte-Carlo (KMC) algorithms.[7] A set of purely classical kinetic equations can be constructed to describe the evolution of the charge population at each molecule,

$$\dot{P}_i = \sum_j \left(k_{ji}P_j - k_{ij}P_i\right). \quad (51)$$

where P_i is the occupation probability of the charge carrier to be on molecule i, and k_{ij} is the charge transfer rate from molecule i to j. Eqn (51) can be solved easily through an iterative numerical scheme: at time zero, the populations $\{P_i\}$ are initialized, *e.g.*, one molecule is set to be unity, while the others are zero.

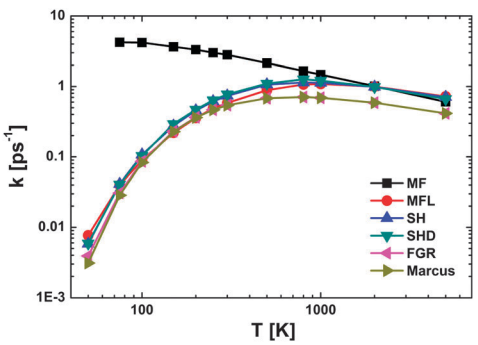

Fig. 5 Temperature dependence of the charge transfer rate in model dimers by the MF approach with and without system-bath interaction (MF and MFL with γ = 4 ps^{-1}), the SH approach with and without decoherence (SH and SHD), together with the reference results from FGR and Marcus formula. The parameters are τ = 50 cm^{-1}, α = 3500 cm^{-1} Å^{-1}, K = 14 500 amu ps^{-2}, and m = 250 amu. Reprinted with permission from ref. 30.

The time evolution of the populations can then be obtained through RK4.[32] The MSD is obtained through

$$\mathrm{MSD}(t) = \sum_i P_i(t)(iL)^2 - \left[\sum_i P_i(t) iL\right]^2. \quad (52)$$

The simulation continues until one gets a linear time dependence of the MSD, and the mobility can be calculated according to eqn (23) and (24). Alternatively, the KMC algorithm approach, which is actually a random walk technique, can be used to simulate the dynamics. In detail, an arbitrary site is initially chosen as the starting position for the charge. For a 1D stack containing only one molecular species, the charge transfer rate to the left neighbor is the same as that to the right one, and thus the charge has a probability of 1/2 to hop left or right. In order to identify the next site for the charge statistically, a random number ζ uniformly distributed between 0 and 1 is generated. If $\zeta < 1/2$, the charge hops to the left neighbor after a waiting time of $1/(2k)$, where k is the intermolecular charge transfer rate; otherwise it hops to the right neighbor. Thousands of realizations should be carried out to obtain the averaged time-dependent MSD and the carrier mobility for equilibrium charge transport.

The small polaron theory is a traditional approach to study charge transport in molecular crystals.[12] Starting from the fully quantum version of the mixed quantum-classical Hamiltonian in eqn (3),[30]

$$\begin{aligned} H &= \sum_k g_1\hbar\omega_1\left(b_{1,k}^+ + b_{1,k}\right)|k\rangle\langle k| \\ &+ \sum_k \left[-\tau + g_2\hbar\omega_2\left(b_{2,k}^+ + b_{2,k}\right)\right](|k\rangle\langle k+1| + |k+1\rangle\langle k|) \\ &+ \sum_k \hbar\omega_1\left(b_{1,k}^+ b_{1,k} + \frac{1}{2}\right) + \sum_k \hbar\omega_2\left(b_{2,k}^+ b_{2,k} + \frac{1}{2}\right), \end{aligned} \quad (53)$$

where $b_{1,k}^{(+)}$ and $b_{2,k}^{(+)}$ are annihilation (creation) operators related to modes $x_{1,k}$ and $x_{2,k}$, respectively. The dimensionless local and nonlocal EPC constants are $g_1 = \alpha(2m_1\hbar\omega_1)^{1/2}/\omega_1$ and $g_2 = \beta(m_2\hbar\omega_2)^{1/2}/\omega_2$. The polaron mobility can be calculated by[13]

$$\mu = \frac{eL^2}{k_B T\hbar^2}\int_{-\infty}^{+\infty} \mathrm{d}t\chi(t)\mathrm{e}^{f(t)}, \quad (54)$$

where

$$\chi(t) = \tau^2 + \frac{1}{2}g_2{}^2\hbar^2\omega_2{}^2\left[(1+n_2)\mathrm{e}^{-i\omega_2 t} + n_2\mathrm{e}^{i\omega_2 t}\right], \quad (55)$$

$$f(t) = \sum_{i=1}^{2} -2g_i{}^2[(1+2n_i)(1-\cos\omega_i t) + i\sin\omega_i t]. \quad (56)$$

n_1 and n_2 are occupation numbers of the two phonon modes.

As expected, the PME and KMC approaches using Marcus charge transfer rates give identical temperature-dependent mobilities (see Fig. 6).[30] When FGR rates are used instead, the mobilities are slightly larger at low temperature due to the quantum effect. The values obtained from small polaron theory are similar to the PME results based on FGR charge transfer rates because both approaches use the same perturbation scheme in the small electronic coupling limit. SH results with or without decoherence are very close and agree very well with the PME or KMC calculations except at high temperatures. The MF mobility using charged geometry gives similar thermally activated temperature dependence but with larger magnitudes especially at low temperatures. In contract, the data obtained from the MF approach with neutral geometry at time zero follow a bandlike power law with temperature, similar to the results shown in Fig. 3 with much larger transfer integrals. With system-bath interactions, the temperature dependence is just up-shifted, showing also bandlike behavior. As a result, the MF theory must be used with caution when studying charge transport in the hopping regime, while the SH approach is generally superior and thus can be exploited to probe the charge transport mechanism in complex situations.[30]

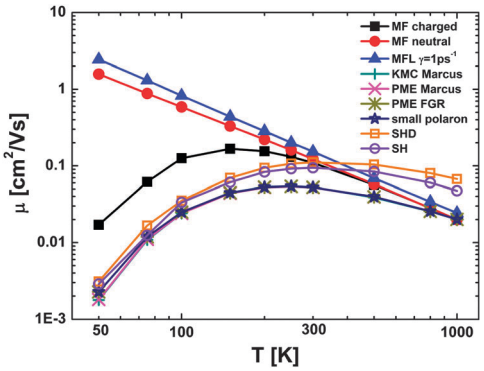

Fig. 6 Temperature dependence of the charge transport mobility in model stacks calculated with the MF theory starting from charged and neutral geometries without system-bath interaction, MF theory with system-bath interaction (MFL, $\gamma = 1\ \mathrm{ps}^{-1}$), the KMC and PME approaches based on Marcus charge transfer rate, the PME approach based on FGR, the small polaron model, and surface hopping calculations with and without decoherence (SHD and SH). Only local electron–phonon couplings are considered. The chosen parameters are $\tau = 50\ \mathrm{cm}^{-1}$, $\alpha = 3500\ \mathrm{cm}^{-1}\ \text{Å}^{-1}$, $K = 14\,500\ \text{amu ps}^{-2}$, and $m = 250$ amu. Reprinted with permission from ref. 30.

3.3 Band-to-hopping crossover

After benchmarking the hopping picture of charge transport, we now investigate to which extent SH approaches can reproduce the band-to-hopping crossover expected upon going from strong to weak coupling regime. The local Hamiltonian has been adopted with the local EPC, α, fixed as $3500\ \mathrm{cm}^{-1}\ \text{Å}^{-1}$. Different values for τ, that is, 50, 100, 200, 400, and 800 cm^{-1}, have been chosen as to cover from weak to strong intermolecular couplings. From Fig. 7, it is clear that the FSH approach successfully reproduces the expected smooth transition from hopping to band-like regimes with the increase of electronic couplings.[29] In detail, the mobility is thermally activated for small τ (50 and 100 cm^{-1}), while it monotonously decreases with temperature for large τ (400 and 800 cm^{-1}). For intermediate electronic couplings around $\tau = 200\ \mathrm{cm}^{-1}$, the carrier mobility is basically insensitive to temperature.

The band-to-hopping crossover phenomenon[52] can be rationalized on the basis of the tendency for the charge carrier to

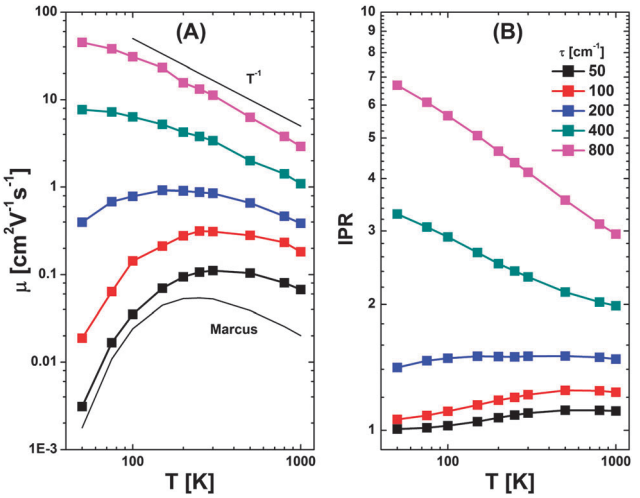

Fig. 7 FSH calculated temperature dependence of the (A) charge mobility and (B) IPR for model stacks. The local Hamiltonian in eqn (1) is used. τ varies as indicated with α = 3500 cm^{-1} Å^{-1}, K = 14 500 amu ps^{-2} and m = 250. The Marcus result and a power law T^{-1} dependence are shown to guide the eyes. Reprinted with permission from ref. 29.

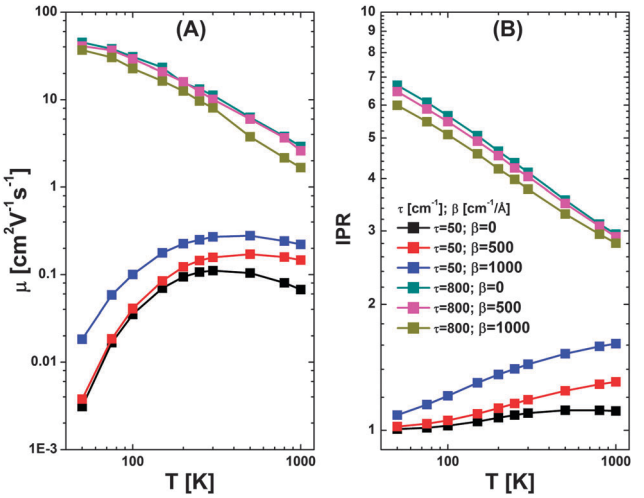

Fig. 8 FSH calculated temperature dependence of the (A) charge mobility and (B) IPR for model stacks. The general Hamiltonian is used. τ and β vary as indicated with α = 3500 cm^{-1} Å^{-1}, K_1 = K_2 = 14 500 amu ps^{-2}, and m_1 = m_2 = 250 amu. Reprinted with permission from ref. 29.

localize in absence of thermal disorder. When temperature is zero, the competition between the local EPCs that tend to localize the charge and the intermolecular couplings that favor charge delocalization result in different charge carrier size. For localized charges, raising the temperature enhances the effect of local EPCs, and induces more fluctuations to the localized charge. The charge carrier has a higher possibility to climb over the barrier, resulting in larger charge delocalization and mobility. In contrast, if the charge is delocalized, any thermal effect from local EPCs tends to destroy the translational symmetry of the electron Hamiltonian, and results in smaller delocalization reflected in a lower mobility. Comparing Fig. 7A with Fig. 7B, there is a strong correlation between the carrier mobility and the charge localization strength (characterized by the inverse participation ratio, IPR).[29] Namely, the charge gets larger (smaller) when the mobility increases (decreases).

3.4 Role of nonlocal electron–phonon couplings

Organic materials are built from weak van der Waals interactions, and thus feature strong nonlocal EPCs, which are key to understand the intrinsic charge transport mechanisms.[27,47] In the literature, disparate views have been advanced regarding the role of nonlocal EPCs on charge transport. It was indicated by Munn and Silbey that incorporating nonlocal EPCs yields higher hopping contribution, which leads to an increase in the charge mobility.[53] In contrast, Troisi pointed out that nonlocal EPCs dynamically localize the charge carrier, and eventually decrease the charge transport efficiency.[27] This 'apparent' divergence has been recently resolved through SH studies.[29]

The role of nonlocal EPCs relies strongly on its interplay with electronic couplings and local EPCs. Special focus has been devoted to its impact on the carrier mobility in both hopping and band regimes.[29] For the sake of convenience, the same force constant and effective mass were chosen for the nuclear vibrations corresponding to both local and nonlocal EPCs. As illustrated in Fig. 8A, FSH calculations revealed that nonlocal EPCs have exactly opposite effects in the two transport pictures: the mobility is increased when accounting for nonlocal EPCs in the hopping scenario but reduced in the band regime.[29] Such an observation is also perfectly in line with the evolution of the charge carrier size (compare Fig. 8A with Fig. 8B). On one hand, nonlocal EPCs introduce perturbations to the localized charge in the hopping picture, aid the charge transfer out of the potential well, and thus enhance charge transport. On the other hand, nonlocal EPCs break the translational symmetry of the electronic Hamiltonian in the band regime, reduce the delocalization strength of charge carriers, and hence decrease the mobility. The results reported by SH thus unify the two distinct pictures proposed by Munn, Silbey[53] and Troisi,[27] which appear as the two limiting cases obtained for hopping and band regimes. It is worthwhile to mention that these findings have been recently confirmed by a fully quantum treatment of charge transport based on the Liouville space hierarchical EOM method.[54]

3.5 Charge transport in realistic materials

For real systems, MQCD studies of charge transport need to couple with first-principles electronic structure calculations. As MQCD deals with the interaction between electrons and nuclei iteratively and stochastically, single point calculations should be carried out repeatedly. Moreover, charge transport is a bulk property, and thus a large supramolecular system needs to be chosen. The associated quantum chemical calculations for the whole system are thus computationally very expansive. As a result, available charge transport studies for realistic materials are quite limited in the literature.

There exits several practical, although maybe appropriate, strategies to investigate the charge transport properties in realistic materials in the framework of MQCD. In the first approach, normal mode or Fourier transform analysis is adopted to

obtain the effective vibrational modes and the associated EPCs, which are further used to parameterize model Hamiltonians and calculate the carrier mobility as described in Sections 3 and 4. This approach has been applied to study charge transport in conjugated polymers,[26,55] molecular crystals,[27,56,57] and discotic liquid crystals.[58] In a second approach feedback from electronic dynamics to nuclear vibrations is neglected. The advantage of this approximation is that charge transport can be studied directly on the basis of *ab initio* electronic structures, going beyond model Hamiltonians. This results in a multiscale strategy: nuclear trajectories are obtained through quantum mechanical or force field molecular dynamics, the time-dependent electronic Hamiltonians are generated from first-principles singlet point calculations, and MQCD simulations are used to calculate the carrier mobility. This type of calculation has been performed for pentathiophene butyric acid monolayers.[46] The third approach takes the advantage of recent developments on fast and efficient electronic structure methods. For instance, MF dynamics has been coupled with density functional tight binding (DFTB)[59] to study the transport properties in a series of donor–acceptor type polymers for photovoltaics.[60] This strategy is advantageous over the other two since quantum backreaction effects are taken into account at the *ab initio* level. Within our knowledge, no extensive calculations of this type have been devoted to SH studies of charge transport which are computationally much more expensive than MF investigations due to the existence of substantial unavoided crossing regimes.[29]

4. Outlook

MQCD techniques have proved to be a powerful tool to study charge transport in organic materials. They are non-perturbative in nature, and can be easily coupled with modern electronic structure methods for atomistic investigations. A lot of insights into the underlying mechanism of charge transport have been obtained with these techniques. The characteristic phenomenon of band-to-hopping crossover in organics has been captured by SH, which has been demonstrated to be superior than MF in general. A quantitative prediction of carrier mobility at the SH level, however, is still a difficult task.

One major difficulty to implement SH dynamics for charge transport is the so-called trivial crossing problem arising due to high degeneracy of electronic levels in large systems. The FSH technique can resolve this issue, but critical parameters are needed to ensure stability and accuracy of the simulations. Parameter-free methods are in demand. Self-consistency checks[61] have been recently proposed to correct the FSSH transition probabilities when encountering surface crossings, providing a straightforward way to describe the trivial crossings. Besides, the fewest switches concept of FSSH has been generalized to gross population flow between states, resulting in the global flux surface hopping (GFSH) method,[24] where the above self-consistency check is automatically satisfied. In contrast to FSSH, GFSH is capable of representing the super-exchange mechanism of charge transport. These new developments can be potentially combined with FSH to generate more reliable and efficient methods for charge transport in large systems. Besides, decoherence is needed for proper description of slow transitions, and thus should be important for low-mobility materials. It would be valuable to incorporate more robust decoherence strategies[43,44,62–65] into further charge transport studies. In addition, the semiclassical treatment of the nuclear tunneling effect should be improved when high-frequency modes play the key role for charge transport. Fully quantum propagation methods, *e.g.*, multilayer multiconfiguration time-dependent Hartree approach,[66,67] can be used.

When mapping model Hamiltonians to realistic materials, we need to evaluate a huge amount of intermolecular electronic couplings, which are computationally very expensive for large systems with many snapshots.[7] Recently, Blumberger's group has proposed a simple computational scheme based on the well-known linear dependence of transfer integral with respect to overlap.[68] Their approach can speed up the calculation by 6 orders of magnitude in comparison with DFT references while keeping high accuracy. For first principle simulations of charge transport, more efficient single point electronic structure methods are needed to further reduce the computational cost. DFTB is a good choice. Semiempirical methods such as Hückel,[69] MNDO[70] and AM1[71] could be also very helpful, although extensive tests are needed.

Acknowledgements

We are grateful for the support from the U.S. National Science Foundation, Grant No. CHE-1300118, for the methods development, and from the U.S. Department of Energy, Grant No. DE-SC0006527, for application studies. The work in Mons was partly supported by the EC 7th Framework Program under Grant Agreement No. 212311 of the ONE-P project, the Inter-university Attraction Pole (IAP 6/27) of the Belgian Federal Science Policy Office, and the Belgian National Fund for Scientific Research (FNRS/FRFC). D.B. is a FNRS Research Director.

References

1 J. E. Anthony, *Chem. Rev.*, 2006, **106**, 5028–5048.
2 N. Koch, *ChemPhysChem*, 2007, **8**, 1438–1455.
3 G. Horowitz, *Adv. Mater.*, 1998, **10**, 365–377.
4 S.-H. Hwang, C. N. Moorefield and G. R. Newkome, *Chem. Soc. Rev.*, 2008, **37**, 2543–2557.
5 Y. Lin, Y. Li and X. Zhan, *Chem. Soc. Rev.*, 2012, **41**, 4245–4272.
6 V. Coropceanu, J. Cornil, D. A. da Silva Filho, Y. Olivier, R. Silbey and J.-L. Brédas, *Chem. Rev.*, 2007, **107**, 926–952.
7 L. Wang, G. Nan, X. Yang, Q. Peng, Q. Li and Z. Shuai, *Chem. Soc. Rev.*, 2010, **39**, 423–434.
8 S. Stafstrom, *Chem. Soc. Rev.*, 2010, **39**, 2484–2499.
9 A. Troisi, *Chem. Soc. Rev.*, 2011, **40**, 2347–2358.
10 Z. Shuai, L. Wang and Q. Li, *Adv. Mater.*, 2011, **23**, 1145–1153.
11 F. Ortmann, F. Bechstedt and K. Hannewald, *Phys. Status Solidi B*, 2011, **248**, 511–525.

12 T. Holstein, *Ann. Phys.*, 1959, **8**, 343.
13 K. Hannewald and P. A. Bobbert, *Appl. Phys. Lett.*, 2004, **85**, 1535–1537.
14 Y.-C. Cheng and R. J. Silbey, *J. Chem. Phys.*, 2008, **128**, 114713.
15 F. Ortmann, F. Bechstedt and K. Hannewald, *Phys. Rev. B: Condens. Matter Mater. Phys.*, 2009, **79**, 235206.
16 L. J. Wang, Q. Peng, Q. K. Li and Z. Shuai, *J. Chem. Phys.*, 2007, **127**, 044506.
17 L. J. Wang, Q. K. Li and Z. Shuai, *J. Chem. Phys.*, 2008, **128**, 194706.
18 S. Hammes-Schiffer, *J. Phys. Chem. A*, 1998, **102**, 10443–10454.
19 A. B. Madrid, K. Hyeon-Deuk, B. F. Habenicht and O. V. Prezhdo, *ACS Nano*, 2009, **3**, 2487–2494.
20 S. A. Egorov, E. Rabani and B. J. Berne, *J. Phys. Chem. B*, 1999, **103**, 10978–10991.
21 P. Ehrenfest, *Z. Phys.*, 1927, **45**, 445–457.
22 O. V. Prezhdo and V. V. Kisil, *Phys. Rev. A: At., Mol., Opt. Phys.*, 1997, **56**, 162–175.
23 J. C. Tully, *J. Chem. Phys.*, 1990, **93**, 1061–1071.
24 L. Wang, D. Trivedi and O. V. Prezhdo, *J. Chem. Theory Comput.*, 2014, **10**, 3598–3605.
25 W. P. Su, J. R. Schrieffer and A. J. Heeger, *Phys. Rev. Lett.*, 1979, **42**, 1698–1701.
26 Å. Johansson and S. Stafström, *Phys. Rev. Lett.*, 2001, **86**, 3602–3605.
27 A. Troisi and G. Orlandi, *Phys. Rev. Lett.*, 2006, **96**, 086601.
28 L. Wang, D. Beljonne, L. Chen and Q. Shi, *J. Chem. Phys.*, 2011, **134**, 244116.
29 L. Wang and D. Beljonne, *J. Phys. Chem. Lett.*, 2013, **4**, 1888–1894.
30 L. Wang and D. Beljonne, *J. Chem. Phys.*, 2013, **139**, 064316.
31 L. Wang, A. V. Akimov, L. Chen and O. V. Prezhdo, *J. Chem. Phys.*, 2013, **139**, 174109.
32 W. H. Press, S. A. Teukolsky, W. T. Vetterling and B. P. Flannery, *Numerical Recipes*, Cambridge University Press, Cambridge, UK, 1992.
33 P. Nettesheim, F. A. Bornemann, B. Schmidt and C. Schütte, *Chem. Phys. Lett.*, 1996, **256**, 581–588.
34 C. Cohen-Tannoudji, B. Diu and F. Laloë, *Quantum Mechanics*, Wiley-Interscience, New York, 1977.
35 A. Einstein, *Ann. Phys.*, 1905, **17**, 549.
36 M. von Smoluchowski, *Ann. Phys.*, 1906, **21**, 756.
37 O. V. Prezhdo and P. J. Rossky, *J. Chem. Phys.*, 1997, **107**, 825–834.
38 E. Neria and A. Nitzan, *J. Chem. Phys.*, 1993, **99**, 1109–1123.
39 S. Fernandez-Alberti, A. E. Roitberg, T. Nelson and S. Tretiak, *J. Chem. Phys.*, 2012, **137**, 014512.
40 E. Hershkovitz, *J. Chem. Phys.*, 1998, **108**, 9253–9258.
41 D. L. Ermak and H. Buckholz, *J. Comput. Phys.*, 1980, **35**, 169–182.
42 V. Chernyak and S. Mukamel, *J. Chem. Phys.*, 2000, **112**, 3572–3579.
43 H. M. Jaeger, S. Fischer and O. V. Prezhdo, *J. Chem. Phys.*, 2012, **137**, 22A545.
44 E. R. Bittner and P. J. Rossky, *J. Chem. Phys.*, 1995, **103**, 8130–8143.
45 A. V. Akimov, A. J. Neukirch and O. V. Prezhdo, *Chem. Rev.*, 2013, **113**, 4496–4565.
46 J. Ren, N. Vukmirović and L.-W. Wang, *Phys. Rev. B: Condens. Matter Mater. Phys.*, 2013, **87**, 205117.
47 L. Wang, Q. Li, Z. Shuai, L. Chen and Q. Shi, *Phys. Chem. Chem. Phys.*, 2010, **12**, 3309–3314.
48 S. H. Lin, C. H. Chang, K. K. Liang, R. Chang, Y. J. Shiu, J. M. Zhang, T. S. Yang, M. Hayashi and F. C. Hsu, *Adv. Chem. Phys.*, 2002, **121**, 1–88.
49 R. A. Marcus, *Rev. Mod. Phys.*, 1993, **65**, 599–610.
50 B. R. Landry and J. E. Subotnik, *J. Chem. Phys.*, 2011, **135**, 191101.
51 H. J. Kreuzer, *Nonequilibrium Thermodynamics and Its Statistical Foundations*, Oxford University Press, New York, 1981.
52 L. B. Schein, C. B. Duke and A. R. McGhie, *Phys. Rev. Lett.*, 1978, **40**, 197–200.
53 R. W. Munn and R. Silbey, *J. Chem. Phys.*, 1985, **83**, 1854–1864.
54 D. Wang, L. Chen, R. Zheng, L. Wang and Q. Shi, *J. Chem. Phys.*, 2010, **132**, 081101.
55 M. Hultell and S. Stafström, *Phys. Rev. B: Condens. Matter Mater. Phys.*, 2007, **75**, 104304.
56 A. Troisi, *Adv. Mater.*, 2007, **19**, 2000–2004.
57 J. Böhlin, M. Linares and S. Stafström, *Phys. Rev. B: Condens. Matter Mater. Phys.*, 2011, **83**, 085209.
58 A. Troisi, D. L. Cheung and D. Andrienko, *Phys. Rev. Lett.*, 2009, **102**, 116602.
59 D. Porezag, T. Frauenheim, T. Köhler, G. Seifert and R. Kaschner, *Phys. Rev. B: Condens. Matter Mater. Phys.*, 1995, **51**, 12947–12957.
60 X. Gao, H. Geng, Q. Peng, J. Ren, Y. Yi, D. Wang and Z. Shuai, *J. Phys. Chem. C*, 2014, **118**, 6631–6640.
61 L. Wang and O. V. Prezhdo, *J. Phys. Chem. Lett.*, 2014, **5**, 713–719.
62 O. V. Prezhdo, *J. Chem. Phys.*, 1999, **111**, 8366–8377.
63 M. D. Hack and D. G. Truhlar, *J. Chem. Phys.*, 2001, **114**, 9305–9314.
64 M. J. Bedard-Hearn, R. E. Larsen and B. J. Schwartz, *J. Chem. Phys.*, 2005, **123**, 234106.
65 J. E. Subotnik and N. Shenvi, *J. Chem. Phys.*, 2011, **134**, 024105.
66 M. H. Beck, A. Jäckle, G. A. Worth and H. D. Meyer, *Phys. Rep.*, 2000, **324**, 1–105.
67 I. R. Craig, M. Thoss and H. Wang, *J. Chem. Phys.*, 2007, **127**, 144503.
68 F. Gajdos, S. Valner, F. Hoffmann, J. Spencer, M. Breuer, A. Kubas, M. Dupuis and J. Blumberger, *J. Chem. Theory Comput.*, 2014, **10**, 4653–4660.
69 E. Hückel, *Z. Phys.*, 1931, **70**, 204.
70 M. J. S. Dewar and W. Thiel, *J. Am. Chem. Soc.*, 1977, **99**, 4899–4907.
71 M. J. S. Dewar, E. G. Zoebisch, E. F. Healy and J. J. P. Stewart, *J. Am. Chem. Soc.*, 1985, **107**, 3902–3909.

